PACS numbers: 42.30.Wb; 42.25.Dd; 87.57.Gg; 87.63.Lk
DOI: 10.1070/QE2001v031n12ABEH002112

Fast approximate statistical nonlinear algorithms for diffusion optical tomography of objects with a complicated internal structure

E V Tret'yakov, V V Shuvalov, I V Shutov

***Abstract*. Fast approximate statistical nonlinear algorithms (capable of real-time operation) for solving direct and inverse problems in the diffusion optical tomography are described. These algorithms were tested by reconstructing a rather complicated internal structure (containing up to three strongly absorbing inclusions no smaller than 5 mm in size) of strongly scattering and weakly absorbing large (up to 140 mm) model objects (with scattering and absorption coefficients equal to 1.4 and 0.005 – 0.015 mm^{-1}, respectively). Experiments were performed using cw radiation of low-power diode lasers (with input power below 20 mW) in the near IR range (between 770 and 820 nm).**

Keywords: *optical tomography, nonlinear algorithms, statistics.*

1. Introduction

Optical tomography (OT) has been developed quite actively in recent years as a new trend in diagnostics. In the OT technique, the object to be diagnosed (henceforth, referred to as the object) is 'illuminated' repeatedly (for various positions of the radiation source and the detector, labelled by the subscripts i and j, respectively) by the input near-IR radiation with known characteristics. These characteristics are the power or energy of the input pulse (from a cw or pulsed source), the duration and the instant of 'incidence' of the pulse on the object, etc. The characteristics of the output radiation such as the power or energy of the output pulse, its shape and its delay relative to the pulse at the input to the object, etc., are measured for all values of i and j.

Measurements for different values of i and j are performed either successively ('scanning') or simultaneously (using multichannel photodetectors and/or radiation sources). The resulting two- or four-dimensional matrix of the output data describes discretely the output radiation characteristics in terms of one (x_i, x_j) or two $(x_i, y_i$ and $x_j, y_j)$ independent coordinates x, y at the surface of the object. The total number of elements of this matrix (N^2 or N^4) is determined by the total number of the positions $i, j = 0, 1, \ldots, N-1$ used for the radiation source and the detector. The output data matrix is then used to reconstruct the internal structure of the object, i.e., the so-called inverse problem is solved. The role of the physical parameters whose spatial distributions are determined (reconstructed) at this stage is played by the absorption and scattering coefficients μ_a and μ_s', the shape of the scattering indicatrix (the anisotropy parameter γ), etc.

It is extremely difficult to solve the inverse problem under the conditions of multiple scattering (the average number of scattering events for photons passing through an object of size $\sim 120 - 150$ mm may be as large as 10^3 or more). However, in the case of small-angle scattering [1 – 5], some of the detected photons have propagated from the point i to the point j almost along rectilinear trajectories [6, 7]. The algorithm for solving the inverse OT problem for such photons can be reduced to the well-studied algorithms used for solving the inverse problem of projection X-ray tomography [8, 9].

For this purpose, we must use certain criteria to select out of the total flux of the photons being detected only a small ('useful') part associated with photons that have passed through the objects along a quite definite type of trajectories (usually, the shortest ones or trajectories of a given length). The existing modifications of the OT technique differ just in the methods used for such a selection, which are realised in the so-called time-domain [10 – 12], coherent [13 – 16] and the frequency-domain [17 – 20] OT.

Note that the use of only a small part of the total flux of photons passing through an object inevitably leads to a sharp decrease in the useful signal and to an increase in the errors. This connects the minimum required power of the input laser radiation (minimum input photon flux), maximum possible size of the object being diagnosed, the minimum time for measurements, and the limiting spatial resolution.

The development of the so-called diffusion OT, in which the entire photon flux passing through the object is detected, allows a considerable simplification and cost-reduction of the tomography equipment. An increase in the output signal results in a drastic decrease in the time of measurements and an increase in the maximum admissible size of the objects being diagnosed. However, the main 'responsibility' of recovering information about the internal structure of the object in this case lies on the algorithms for solving the inverse problem, which should be applicable under conditions of multiple scattering.

In the currently available methods of solving the inverse problem (the diffusion equation method [21, 22], the Bayes

E V Tret'yakov, V V Shuvalov, I V Shutov International Teaching and Research Laser Center, M V Lomonosov Moscow State University, Vorob'evy gory, 119899 Moscow, Russia

Received 3 August 2001
Kvantovaya Elektronika **31** (12) 1095 – 1100 (2001)
Translated by Ram Wadhwa

method [23, 24], the gradient iterative techniques [25, 26], the 'mean trajectories' method [27–29], etc.), the time of reconstruction of the internal structure of the object increases drastically for objects of size ~ 150 mm, when the number of scattering events attains the value $\sim 10^3$ or more. Because the equipment used for tomography allows the necessary measurements to be completed in just a few minutes [30–32], it is necessary to develope approximate algorithms allowing the reconstruction of the internal structure of the object for nearly the same time.

In this work, we consider one of the fast approximate nonlinear statistical algorithms for solving direct and inverse problems of diffusion OT, and present the first results of its experimental verification.

2. First iteration of the algorithm for fast solution of the inverse problem

For a fast reconstruction of the internal structure of an object, an approximate nonlinear statistical algorithm was proposed in Refs. [30–32] for solving the inverse OT problem. In this algorithm, it is assumed that the difference in the photon fluxes of the output radiation $\Phi_{i,j}^{(1)}$ in the absence of spatial inhomogeneities (absorbing and/or scattering 'inclusions') and $\Phi_{i,j}$ in the presence of such inhomogeneities is due just to their emergence. It is assumed that the probability $P_{i,j}^{(1)}$ of finding inclusions in an object from the results of the i, j measurements is proportional to $\Phi_{i,j}^{(1)} - \Phi_{i,j}$, while the spatial distribution of $P_{i,j}^{(1)}$ is determined by the three-dimensional probability density $p_{i,j}^{(1)}(\boldsymbol{r}) \propto P_{i,j}^{(1)} f_{i,j}^{(1)}(\boldsymbol{r})$, where $f_{i,j}^{(1)}(\boldsymbol{r})$ is the three-dimensional distribution of the probability of passing through a point with coordinate $\boldsymbol{r}$ in the object for photons detected in the i, j measurements. The reconstructed internal structure is described by the complete three-dimensional distribution of the probability $p_{\Sigma}^{(1)}(\boldsymbol{r})$ of finding the inclusions at various points in the object, which is defined in terms of the product $\prod_{i,j} P_{i,j}^{(1)} f_{i,j}^{(1)}(\boldsymbol{r})$ from the results of N^2 or N^4 (see above) independent measurements ('realisations'). The information required *a priori* for the working of the algorithm [$\Phi_{i,j}^{(1)}$ and $f_{i,j}^{(1)}(\boldsymbol{r})$] is also calculated approximately by using the following empirical (in real or numerical experiments) dependence for 'spatially homogeneous' objects (in the absence of inclusions, for $\mu_a, \mu_s' = \text{const}$):

$$\Phi_{i,j}^{(1)} \propto P L_{i,j}^{-2} \exp(-\mu_a \xi L_{i,j}) \tag{1}$$

and by taking into account the possibility of scaling of the unique 'standard' three-dimensional distribution $f_L(\boldsymbol{r})$ by varying the separation $L_{i,j}$ between the radiation source and the detector. Here, P is the power of the input radiation, $\xi = \xi(\mu_a, \mu_s')$ is a parameter describing the 'average elongation' of the trajectories of the photons being detected relative to $L_{i,j}$; and $f_L(\boldsymbol{r})$ is the three-dimensional distribution of the probability of passage of photons through a homogeneous object, L being the separation between the radiation source and the detector. For spherical and cylindrical objects subjected to diagnosis, $L_{i,j} = 2R \times \sin(\alpha_{i,j}/2)$, where R is the radius of the object and $\alpha_{i,j}$ is the central angle between the positions of the radiation source and the detector.

Fig. 1 shows the schematic diagram of the algorithm for a fast approximate computation of $f_{i,j}^{(1)}(\boldsymbol{r})$. The three-dimensional distribution $f_L(\boldsymbol{r})$ is calculated by the Monte Carlo method and is approximated by the three-dimensional distribution with Gaussian cross sections ('standard three-dimensional distribution approximation' block). The 'scaling' and 'rotation' blocks execute the necessary geometrical transformations of the results of approximation, recalculating $f_L(\boldsymbol{r}) \to f_{L_{i,j}}(\boldsymbol{r})$ for $L \to L_{i,j}$ and 'connecting' the beginning and the end of each of the obtained three-dimensional distributions $f_{i,j}^{(1)}(\boldsymbol{r})$ with the points i and j. Because the Monte Carlo simulation carried out by us showed that for $\alpha_{i,j} \neq 180^\circ$, the axes ('generatrices') of the three-dimensional distributions $f_{i,j}^{(1)}(\boldsymbol{r})$ deviated from straight lines connecting the points i and j due to the boundary conditions, such deviations were taken into account by the 'generatrix shape correction' block, which performed the required 'bending' of the three-dimensional distributions $f_{i,j}^{(1)}(\boldsymbol{r})$. The shape of their generatrices is defined by parabolas whose 'deflection' depends on $\alpha_{i,j}$.

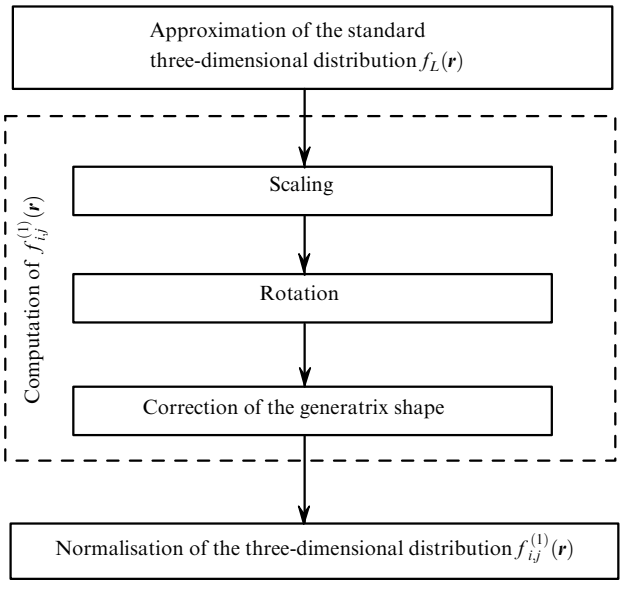

Figure 1. Algorithm for approximate calculation of three-dimensional distributions $f_{i,j}^{(1)}(\boldsymbol{r})$ for a strongly scattering 'spatially homogeneous' object.

Finally, the 'three-dimensional distribution normalisation' block performs the final transformations of $f_{i,j}^{(1)}(\boldsymbol{r})$ by normalising the photon flux detected in each cross section (perpendicular to the genereatrix) of $f_{i,j}^{(1)}(\boldsymbol{r})$ to a constant defined by formula (1). The results of the algorithm operation, which requires not more than 30 s for obtaining an array of 1024 three-dimensional distributions ($0 \leqslant i, j \leqslant 31$) on a PIII-800 PC, are presented in Fig. 2 showing the results of 'exact' (Monte Carlo) and approximate calculation of $f_{i,j}^{(1)}(\boldsymbol{r})$ for $\alpha = 180^\circ$ and 90°.

3. Second iteration of the algorithm for fast solution of the inverse problem

The experimental verification of the fast approximate statistical algorithm described above was reported earlier in Refs [30–32] by reconstructing the position and shape of a strongly absorbing inclusion of diameter down to 5 mm in a strongly scattering model object of diameter up to 140 mm. This algorithm is found to be equally 'successful'

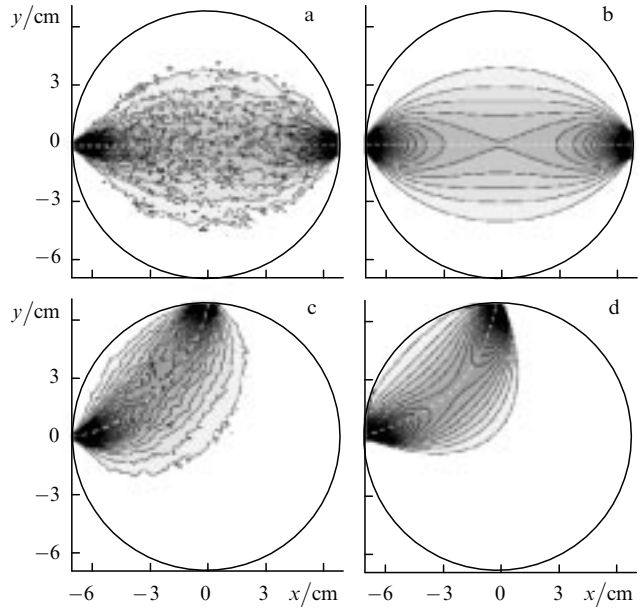

Figure 2. Results of the exact Monte Carlo (a, c) and approximate (b, d) calculations of three-dimensional distributions $f_{i,j}^{(1)}(\boldsymbol{r})$ for a strongly scattering 'homogeneous' object. The depth of darkening is proportional to the probability of passage of the detected phonons; the central angle $\alpha_{i,j}$ between the positions of the radiation source and the detector is 180 (a, b) and 90° (c, d).

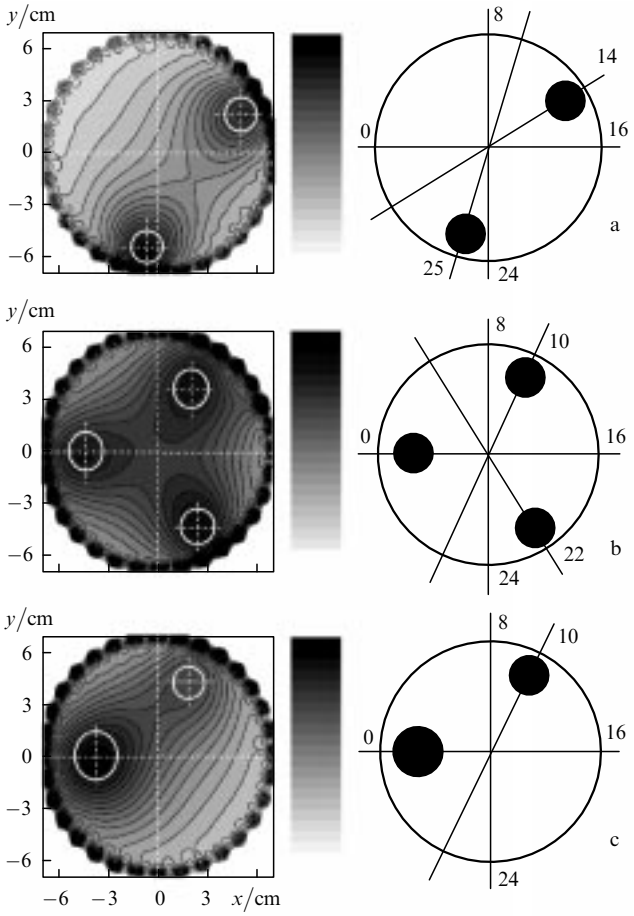

Figure 3. Reconstructed inner structure $p_{\Sigma}^{(1)}(\boldsymbol{r})$ of a model object of diameter 140 mm (left) and the corresponding experimental geometry (right) for two (a, c) and three (b) strongly absorbing inclusions of identical (a, b) and different (c) diameters. The depth of darkening is proportional to the logarithm of the absorption coefficient, and the numbers on the circles correspond to the values of i or j.

in solving the problem of reconstructing the internal structure of an object containing two or three strongly absorbing inclusions of the same size (Fig. 3). However, our subsequent experiments showed that the above algorithm was no longer efficient even in the simplest case when the model object contained two strongly absorbing inclusions of different sizes. This is due to the nonlinearity associated with the description of the reconstructed internal structure of the object by the three-dimensional probability density $p_{\Sigma}^{(1)}(\boldsymbol{r}) \propto \prod_{i,j} P_{i,j}^{(1)}\, f_{i,j}^{(1)}(\boldsymbol{r})$ of finding the inclusions for different values of $\boldsymbol{r}$. It is this nonlinearity that leads to the classical 'impasse' situation for nonlinear problems in which the 'winner takes all', and only the most 'salient' features of the internal structure of the object are reconstructed.

The above difficulty can be removed by introducing the second iteration in the algorithm proposed in Refs. [30–32] for solving the inverse problem. The internal structure of the object $p_{\Sigma}^{(1)}(\boldsymbol{r})$ reconstructed at the first iteration (obtained in accordance with the algorithm described above) is used for the fast approximate computation of *a priori* information $\Phi_{i,j}^{(2)}$ and $f_{i,j}^{(2)}(\boldsymbol{r})$ for the second iteration. It is assumed that the difference in the photon fluxes of the output radiation in the presence of the reconstructed parts $p_{\Sigma}^{(1)}(\boldsymbol{r})$ $(\Phi_{i,j}^{(2)})$ of the internal structure and $(\Phi_{i,j})$ in the real experiment is due only to the reconstruction errors, and the total probability of finding such errors in the i, j measurements is $P_{i,j}^{(2)} \propto \Phi_{i,j}^{(2)} - \Phi_{i,j}$.

It is assumed that the spatial distribution of $P_{i,j}^{(2)}$ is determined by the three-dimensional probability density $p_{i,j}^{(2)}(\boldsymbol{r}) \propto P_{i,j}^{(2)} f_{i,j}^{(2)}(\boldsymbol{r})$, where $f_{i,j}^{(2)}(\boldsymbol{r})$ is the three-dimensional distribution of the probability of the passage of photons detected in the i, j measurement through a 'spatially inhomogeneous' $(\mu_a, \mu_s' \neq \text{const})$ object with an internal structure defined by the three-dimensional distribution of $p_{\Sigma}^{(1)}(\boldsymbol{r})$. The details of the internal structure reconstructed at the second iteration are described by the total three-dimensional probability density $p_{\Sigma}^{(2)}(\boldsymbol{r})$, which is also determined from all the N^2 or N^4 (see above) measurements through the product $\prod_{i,j} P_{i,j}^{(2)} f_{i,j}^{(2)}(\boldsymbol{r})$. In the iterative algorithm for the reconstruction of the internal structure of an object, the structure is described by a linear superposition $p_{\Sigma}(\boldsymbol{r}) = p_{\Sigma}^{(1)}(\boldsymbol{r}) + p_{\Sigma}^{(2)}(\boldsymbol{r})$, while the solution of the inverse problem is transformed only insignificantly (Fig. 4). Further iterations can be included in the above-mentioned algorithm if required.

4. Algorithm for fast solution of the direct problem

However, the realisation of the iterative algorithm for solving the inverse problem according to the scheme described in Fig. 4 requires a fast computation of *a priori* information $\Phi_{i,j}^{(2)}$ and $f_{i,j}^{(2)}(\boldsymbol{r})$ for the second iteration. In other words, we should 'learn' to solve the direct OT problem quickly. It turns out that the possibility of scaling of the three-dimensional distributions in a homogeneous object allows the construction of a fast algorithm for approximate solution of this problem also in the case when the strongly scattering object subjected to diagnosis contains absorbing inclusions. Fig. 5 illustrates the scheme of such an algorithm, which is a natural extension of the 'excision'

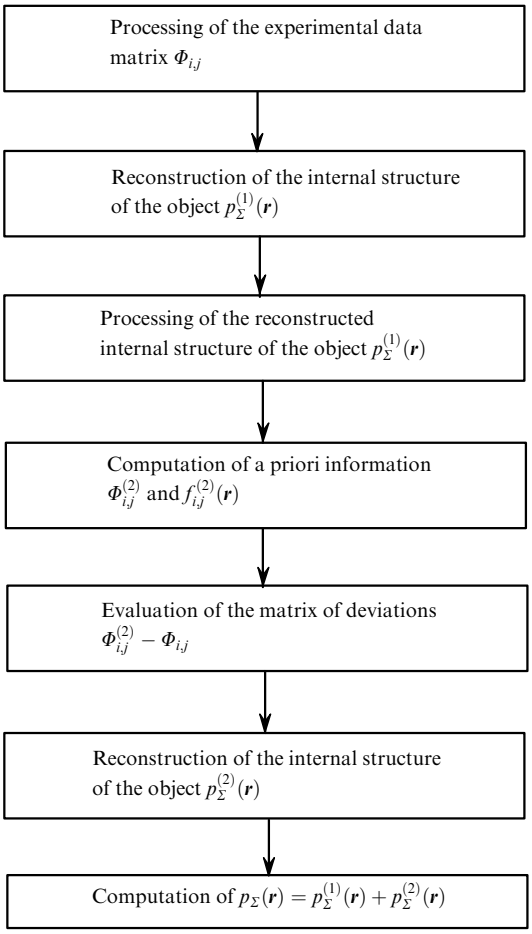

Figure 4. Iterative algorithm for solving the inverse problem for a strongly scattering object with a complex internal structure.

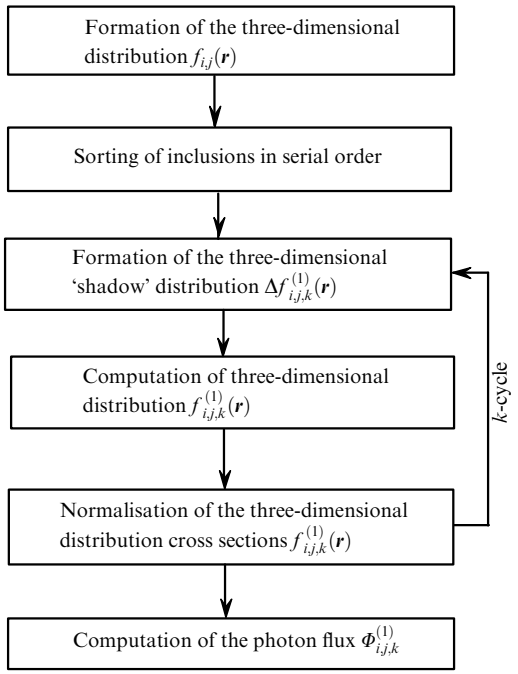

Figure 5. Algorithm of approximate computation of three-dimensional distributions $f_{i,j,k}^{(1)}(\boldsymbol{r})$ for a strongly scattering 'inhomogeneous' object with a complicated internal structure (i and j correspond to the input and output points for the radiation; k is the inclusion number).

method proposed in Refs [30–32] and is based on the linearity of the initial problem.

The probability for the detected photons to pass through any cross section of any three-dimensional distribution $f_{i,j}(\boldsymbol{r})$ is always the same because these photons were obviously not absorbed. Therefore, the appearance of a strongly absorbing inclusion in a homogeneous object will result in the absorption of a certain part $\Delta\Phi_{i,j,1}^{(1)}$ of the photon flux $\Phi_{i,j}^{(1)}$, which therefore, will not be detected in the i, j measurement. In the first approximation, the relative fraction of the 'vanishing' part $\Delta\Phi_{i,j,1}^{(1)}/\Phi_{i,j}^{(1)}$ of the flux $\Phi_{i,j}^{(1)}$ in each dimension can be determined by 'excising' the appropriate part (three-dimensional distribution of the 'shadow') $f_{i,j,1}^{(1)}(\boldsymbol{r})$ of the corresponding cross sections $f_{i,j}^{(1)}(\boldsymbol{r})$.

If the object contains $n > 1$ absorbing inclusions, the computational algorithm becomes somewhat more complicated and acquires an iterative form. While calculating the relative fraction $\Delta\Phi_{i,j,k}^{(1)}/\Phi_{i,j,k-1}^{(1)}$ of the part excised by the kth inclusion from the flux $\Phi_{i,j}^{(1)}$, which should arrive at the photodetector in the i, j measurement, we use the flux

$$\Phi_{i,j,k-1}^{(1)} = \Phi_{i,j}^{(1)} - \sum_{m=1}^{k-1} \Delta\Phi_{i,j,m}^{(1)}$$

and the three-dimensional distribution

$$f_{i,j,k-1}^{(1)}(\boldsymbol{r}) = f_{i,j}^{(1)}(\boldsymbol{r}) - \sum_{m=1}^{k-1} \Delta f_{i,j,m}^{(1)}(\boldsymbol{r}),$$

corresponding to the same measurement in the case of a homogeneous object for the $(k-1)$th inclusion. For the sake of unification of the system of notation, it was assumed above that $\Phi_{i,j,0}^{(1)} = \Phi_{i,j}^{(1)}$ and $f_{i,j,0}^{(1)}(\boldsymbol{r}) = f_{i,j}^{(1)}(\boldsymbol{r})$.

While employing the above-mentioned iterative algorithm for an approximate solution of the direct problem, we must determine for each set of i, j the sequential order of all $n > 1$ inclusions and carry out successive approximate computations of the three-dimensional distributions $\Delta f_{i,j,k}^{(1)}(\boldsymbol{r})$ $(1 \leqslant k \leqslant n)$ of the 'shadows' corresponding to these inclusions. The diffusive nature of photon propagation in the object is taken into account in the calculation of $\Delta f_{i,j,k}^{(1)}(\boldsymbol{r})$. As a matter of fact, the above-mentioned possibility of geometrical scaling of the same 'standard' distribution $f_L(\boldsymbol{r})$ is used in this case. For each iteration during all the transformations, the photon flux $\Phi_{i,j,k}^{(1)}$ being detected is maintained constant in all cross sections of the corresponding three-dimensional distributions $f_{i,j,k}^{(1)}(\boldsymbol{r})$.

Fig. 6 shows the result of the algorithm operation, which takes less than two minutes on a PIII-800 PC for the formation of arrays of 1024 $(0 \leqslant i, j \leqslant 31)$ fluxes $\Phi_{i,j}^{(2)} = \Phi_{i,j,3}^{(1)}$ and three-dimensional distributions $f_{i,j}^{(2)}(\boldsymbol{r}) = f_{i,j,3}^{(1)}(\boldsymbol{r})$ in an object with three inclusions. One can see that the results of 'exact' (Monte Carlo) and approximate computations of the three-dimensional distributions $f_{i,j}^{(2)}(\boldsymbol{r})$ for an object with a strongly absorbing inclusion are in fairly good agreement for $\alpha_{i,j} = 180^{\circ}$. The flux distribution $\Phi_{i,j}^{(2)}$ for the detected photons obtained in a real experiment for an object with three strongly absorbing inclusions is consistent with the results of approximate calculations.

5. Reconstruction of the 'fine' details of the internal structure of an object

The reconstruction of the internal structure of a strongly scattering homogeneous object (i.e., the three-dimensional

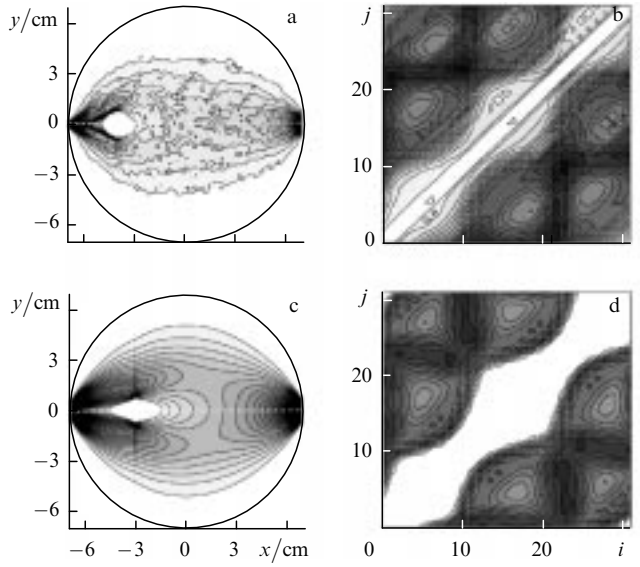

Figure 6. Three-dimensional distributions of $f^{(1)}_{i,j,1}(\boldsymbol{r})$ for an object with a strongly absorbing inclusions calculated by the exact Monte Carlo method (a) and by the approximate method (c), and the photon flux $\Phi^{(1)}_{i,j,3}$ detected in the presence of three inclusions in the geometry of Fig. 3b for the real experiment (b) and the approximate calculation (d). The depth of darkening is proportional to the logarithm of the flux, and the numbers i and j correspond to the input and output points for the radiation.

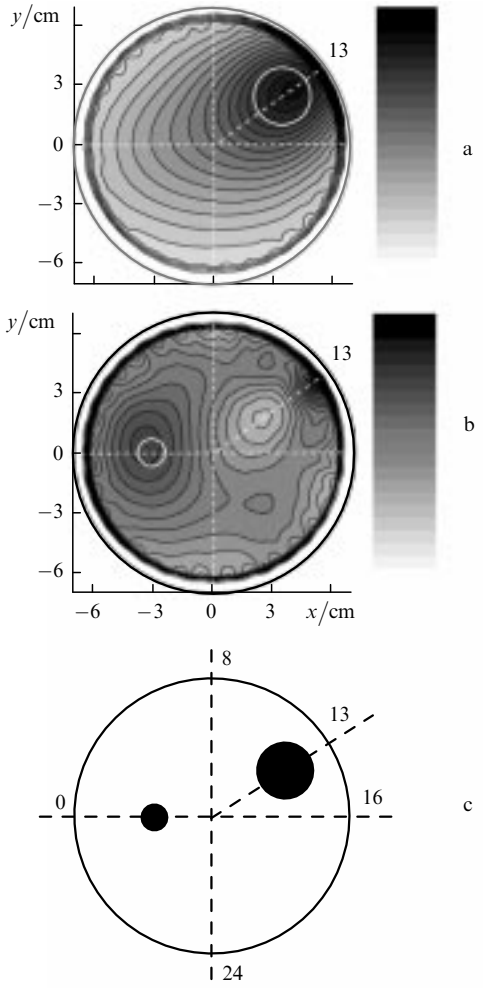

Figure 7. Reconstructed inner structure of a model object of diameter 140 mm with two strongly absorbing inclusions of different diameters after the first ($p^{(1)}_{\Sigma}(\boldsymbol{r})$, a) and second ($p^{(2)}_{\Sigma}(\boldsymbol{r})$, b) iterations, and the experimental geometry (c). The depth of darkening is proportional to the logarithm of the absorption coefficient; numbers on the circles correspond to the values of i or j.

distribution $p_{\Sigma}(\boldsymbol{r})$ of the probability of finding inclusions) with two strongly absorbing inclusions of noticeably different sizes from an array of 1024 ($0 \leqslant i, j \leqslant 31$) measurement of fluxes $\Phi_{i,j}$ takes less than two minutes on a PIII-800 PC with the help of the above-mentioned iterative algorithm. Fig. 7 shows the results of such a reconstruction based on the data obtained in real experiments. One can easily verify that only the 'image' of the larger inclusion is observed in the reconstructed three-dimensional distribution of $p^{(1)}_{\Sigma}(\boldsymbol{r})$ at the first iterative stage of the algorithm. However, the image of the smaller inclusion also appears in the reconstructed three-dimensional distribution of $p^{(2)}_{\Sigma}(\boldsymbol{r})$ at the second iteration. The image of the larger inclusion is almost completely 'subtracted' at this stage, which indirectly confirms the high degree of accuracy of the approximate computational technique employed by us.

6. Conclusions

We are certainly not in a position to provide a rigorous substantiation of the fast approximate statistical nonlinear algorithms (capable of real-time operation) described above for solving the direct and inverse problems of diffusion OT. However, we believe that the schematic construction and the structure of these algorithms reflects quite clearly the probabilistic nature of the propagation of photons through strongly scattering objects of size larger than the so-called transport scattering length $(\mu'_{\mathrm{s}})^{-1}$.

The above results of testing these algorithms by considering the reconstruction of rather complicated internal structures (as compared to those considered in Refs [30–32]) (up to three strongly absorbing inclusions of size at least 5 mm) of strongly scattering and weakly absorbing objects (the scattering coefficient $\mu'_{\mathrm{s}} = 1.4\ \mathrm{mm}^{-1}$ and the absorption coefficient $\mu_{\mathrm{a}} = 0.005 - 0.015\ \mathrm{mm}^{-1}$) of quite a large size (140 mm) also confirm the efficiency of these algorithms. It is important from the practical point of view that we used in all experiments inexpensive low-power (input power below 20 mW) cw diode lasers emitting in the near IR range between 770 and 820 nm.

Acknowledgements. This work was supported by the Russian Foundation for Basic Research (Grants Nos 00-15-96726 and 01-02-17305)

References

1. *Photon Propagation In Tissues, Proc. SPIE Int. Soc. Opt. Eng.* **2626** (1996)
2. *Photon Propagation In Tissues II, Proc. SPIE Int. Soc. Opt. Eng.* **2925** (1996)
3. *Photon Propagation In Tissues III, Proc. SPIE Int. Soc. Opt. Eng.* **3194** (1998)
4. *Photon Propagation In Tissues IV, Proc. SPIE Int. Soc. Opt. Eng.* **3566** (1998)
5. *Photon Migration in Tissues*, Chance B (Ed.) (New York: Plenum Press, 1989)

6. Ho P P, et al. *Opt. Photon. News* **4** 23 (1993)
7. Feng S, et al. *Proc. SPIE Int. Soc. Opt. Eng.* **1888** 78 (1993)
8. Herman G T *Image Reconstruction from Projections: The Fundamentals of Computerized Tomography* (San Francisco: Academic Press, 1980)
9. *Basic Methods of Tomography and Inverse Problems: A Set of Lectures*, Sabatier P C (Ed.) (Bristol: Adam Hilger, 1987)
10. Wang L et al. *Science* **253** 769 (1991)
11. Proskurin S G et al. *Proc. SPIE Int. Soc. Opt. Eng.* **2389** 157 (1995)
12. Wells K et al. *Proc. SPIE Int. Soc. Opt. Eng.* **2979** 599 (1997)
13. Hee M R et al. *Optical Coherence Tomography of Ocular Diseases* (Thorofare: Slack Inc., 1996)
14. *CIS selected papers: Coherence-domain Methods in Biomedical Optics. Proc. SPIE Int. Soc. Opt. Eng.* **2732** (1996)
15. Tearney G J et al. *Proc. SPIE Int. Soc. Opt. Eng.* **2389** 29 (1995)
16. *Coherent Domain Methods in Biomedical Science and Clinical Applications IV, Proc. SPIE Int. Soc. Opt. Eng.* **3915** (2000)
17. O'Leary M A et al. *Opt. Lett.* **20** 426 (1995)
18. Papaioannou D G et al. *Proc. SPIE Int. Soc. Opt. Eng.* **2626** 218 (1995)
19. Bocher T et al. *Proc. SPIE Int. Soc. Opt. Eng.* **2626** 283 (1995)
20. Sevick-Muraca E M et al. *SPIE Institutes for Advanced Optical Technologies. Ser.* (Bellingham, WA, 1993), Vol. 11, p. 485
21. Markel V A, Schotland J C *J. Opt. Soc. Am. A* **18** 1336 (2001).
22. Gryazin Y A et al. *Inverse Problems* **15** 373 (1999)
23. Jong C, et al. *J. Opt. Soc. Am. A* **16** 2400 (1999)
24. Millane R P, et al. *Proc. SPIE Int. Soc. Opt. Eng.* **4123** 295 (2000)
25. Hielscher A H, Bartel S *Proc. SPIE Int. Soc. Opt. Eng.* **3979** 575 (2000)
26. Hielscher A H, Bartel S *Proc. SPIE Int. Soc. Opt. Eng.* **4160** 118 (2000)
27. Lyubimov V V, et al. *Proc. SPIE Int. Soc. Opt. Eng.* **3566** 57 (1998)
28. Lyubimov V V, et al. *Proc. SPIE Int. Soc. Opt. Eng.* 3816 183 (1999)
29. Volkonskii V B et al. *Opt. Spektr.* **87** 457 (1999)
30. Chursin D A et al. *Kvantovaya Electron.* **29** 83 (1999) [*Quantum Electron.* **29** 921 (1999)].
31. Shuvalov V V et al. *Laser Physics* **11** 636 (2001)
32. Malikov E V *Kvantovaya Electron.* **30** 78 (2000) [*Quantum Electron.* **30** 78 (2000)].